



Contents lists available at ScienceDirect

Applied Surface Science

journal homepage: [www.elsevier.com/locate/apsusc](http://www.elsevier.com/locate/apsusc)



# Impact of strain on the passivation efficiency of Ge dangling bond interface defects in condensation grown $\text{SiO}_2/\text{Ge}_x\text{Si}_{1-x}/\text{SiO}_2/(1\ 0\ 0)\text{Si}$ structures with nm-thin $\text{Ge}_x\text{Si}_{1-x}$ layers

O. Madia<sup>a,\*</sup>, A.P.D. Nguyen<sup>a</sup>, N.H. Thoan<sup>a</sup>, V. Afanas'ev<sup>a</sup>, A. Stesmans<sup>a</sup>, L. Souriau<sup>b</sup>, J. Slotte<sup>c</sup>, F. Tuomisto<sup>c</sup>

<sup>a</sup> Department of Physics and Astronomy, University of Leuven, Celestijnenlaan 200D, B-3001 Leuven, Belgium

<sup>b</sup> IMEC, Kapeldreef 75, B-3001 Leuven, Belgium

<sup>c</sup> Department of Applied Physics, Aalto University School of Science, P.O. Box 11100, FI-00076 Aalto, Finland

## ARTICLE INFO

Available online xxx

## ABSTRACT

Hydrogen passivation of germanium dangling bond defects observed as paramagnetic  $\text{GeP}_{b1}$  centers at the  $\text{Ge}_x\text{Si}_{1-x}/\text{SiO}_2$  interfaces is studied as a function of Ge concentration and thickness of the  $\text{Ge}_x\text{Si}_{1-x}$  layer. By correlating the results obtained by three independent defect-sensitive methods – electron spin resonance spectroscopy, ac conductance of the  $\text{Ge}_x\text{Si}_{1-x}$  layer, and the positron annihilation spectroscopy – with the results of strain measurements by high-resolution X-ray diffractometry, we found that the density of the Ge dangling bonds reflects residual strain in the  $\text{Ge}_x\text{Si}_{1-x}$  layer. Furthermore, in the layers with high strain the hydrogen passivation efficiency of dangling bonds is found to decrease, suggesting a considerable spread in the activation energies of the passivation/depasivation reactions.

© 2013 Elsevier B.V. All rights reserved.

## 1. Introduction

Germanium–silicon  $\text{Ge}_x\text{Si}_{1-x}$  alloys provide a unique possibility to attain a higher, as compared to silicon, mobility in the metal–oxide–semiconductor (MOS) transistor channel while retaining the processing flow of the highly successful Si MOS technology. Furthermore, the mobility may be additionally enhanced by introducing strain into the channel region promising a boost in the drain current. However, application of  $\text{Ge}_x\text{Si}_{1-x}$  as a channel semiconductor faces the problem of substantial densities of semiconductor/oxide interface traps, of which the atomic origin and electrical behavior remain largely unknown. With respect to the interfaces of silicon with thermally grown  $\text{SiO}_2$ , it is well known that defects associated with dangling bonds (DBs) of Si atoms provide the dominant contribution to the observed density of interface traps [1]. As to the interfaces of pure Ge with deposited oxides, no measurable contribution of conventional Ge DB defects to the interface trap density has been found at interfaces of Ge with  $\text{HfO}_2$  and  $\text{Al}_2\text{O}_3$  [2,3]. In agreement with these inferences, Ge/Ge-oxide interface trap densities in the low  $10^{11}\text{ cm}^{-2}\text{ eV}^{-1}$  range have been reported [4]. At the same time, the presence of a system of DB defects at the Ge/Ge-oxide interface has been demonstrated by electrically-detected spin resonance, without, however, providing an estimate

of their density [5]. By contrast, the presence of a substantial density of Ge DB-type centers at interfaces of condensation-grown  $\text{Ge}_x\text{Si}_{1-x}$  with  $\text{SiO}_2$ , typified as  $\text{GeP}_{b1}$  defects, [6,7] has been firmly exposed by conventional electron spin resonance (ESR) observations and correlated with electrical results [8]. This raises the important point about the possibility to passivate traps at interfaces of Ge and  $\text{Ge}_x\text{Si}_{1-x}$  by annealing in molecular hydrogen, which has been the basic approach to attain device-grade Si/SiO<sub>2</sub> interfaces.

In the present study we have investigated the Ge DBs in the  $\text{SiO}_2/\text{Ge}_x\text{Si}_{1-x}/\text{SiO}_2$  structures and their passivation by annealing in molecular hydrogen as influenced by residual strain in the  $\text{Ge}_x\text{Si}_{1-x}$  layer. By combining three spectroscopic methods of defect analysis with X-ray diffractometry measurements we found that the highest strain, extensively studied in the literature [9,10], results in the highest initial density of the Ge DB defects. Moreover, in the samples with the highest strain, the efficiency of passivating the DB centers by  $\text{H}_2$  is dramatically reduced, leaving a considerable fraction of defects unpassivated, i.e., in the electrically active state. The latter suggests large site-to-site variations in activation energies for the passivation/depasivation reactions.

## 2. Experimental

### 2.1. Sample preparation

In this work we addressed  $\text{Ge}_x\text{Si}_{1-x}$  layers prepared on Si wafers using the condensation growth technique, which allows one to

\* Corresponding author Tel.: +32 476097872.

E-mail addresses: [oreste.madia@fys.kuleuven.be](mailto:oreste.madia@fys.kuleuven.be), [orestemadia@gmail.com](mailto:orestemadia@gmail.com) (O. Madia).

**Table 1**  
Composition and thickness of the  $\text{Ge}_x\text{Si}_{1-x}$  layer reached in the various samples fabricated by the Ge condensation technique starting from different initial  $\text{Ge}_x\text{Si}_{1-x}$  layers.

104 nm $\text{Ge}_{0.27}\text{Si}_{0.73}$				64 nm $\text{Ge}_{0.24}\text{Si}_{0.76}$			
No.	Ge fraction $x$	$\text{Ge}_x\text{Si}_{1-x}$ layer thickness [nm]	TOX thickness [nm]	No.	Ge fraction $x$	$\text{Ge}_x\text{Si}_{1-x}$ layer thickness [nm]	TOX thickness [nm]
1	0.45	54	150	6	0.28	64	84
2	0.58	57	170	7	0.42	34	120
3	0.70	46	195	8	0.55	27	135
4	0.73	45	195	9	0.65	24	148
5	0.93	27	210	10	0.75	16	155
				11	0.87	15	158

integrate  $\text{Ge}_x\text{Si}_{1-x}$  materials into large-area silicon wafers directly. The studied  $\text{SiO}_2/\text{Ge}_x\text{Si}_{1-x}/\text{SiO}_2$  heterostructures were prepared on 200 mm diam. silicon-on-insulator (SOI) wafers with a 22 nm thick boron doped ( $5 \times 10^{17}$  atoms/cm<sup>3</sup>) top Si layer and a buried oxide (BOX) layer of 140 nm thickness. After a clean in a 2% HF aqueous solution and an 850 °C bake in  $\text{H}_2$  at reduced pressure, a Si-rich  $\text{Ge}_x\text{Si}_{1-x}$  ( $x = 0.24\text{--}0.27$ ) layer was deposited using  $\text{SiH}_4$  and  $\text{GeH}_4$  as precursors in a ASM Epsilon® 2000 reactor. After the growth of a thin (7 nm) epi-Si layer on top, which was needed to prevent outdiffusion of Ge during the early stage of the thermal oxidation process, the structure was subjected to three steps of dry oxidation (1150, 1000 and 900 °C), each followed by annealing in inert (Ar) ambient. The high temperatures employed (>1000 °C) prevents the formation of a stable Ge oxide and only  $\text{SiO}_2$  was formed at the interface, thus leading to a gradual Ge enrichment of the starting layer. Cross-sectional TEM images of the heterostructures, as well as further details regarding the fabrication technique, can be found in the literature [10,11].

Using different initial thicknesses of the  $\text{Ge}_x\text{Si}_{1-x}$  layer and different condensation thermal budgets, two sets of samples were prepared for reasons of comparison (see Table 1); a lowest  $\text{Ge}_x\text{Si}_{1-x}$  final thickness of 15 nm is achieved.

## 2.2. Characterization techniques

Structural characterization, aimed in particular at the determination of the  $\text{Ge}_x\text{Si}_{1-x}$  layer thickness and of the residual strain induced on the  $\text{Ge}_x\text{Si}_{1-x}$  layer by thermal oxidation of silicon, was performed using high-resolution X-ray diffractometry (HR-XRD). The measured lattice constant has been plotted as a function of the Ge atomic fraction  $x$ , experimentally determined by Rutherford backscattering spectrometry (RBS), and compared to the expected lattice constant of the unstrained (relaxed)  $\text{Ge}_x\text{Si}_{1-x}$  alloy of the same composition. The difference between these lattice constants was taken as the measure of the residual strain in the condensation grown  $\text{Ge}_x\text{Si}_{1-x}$  layer.

Electrical characterization was performed by means of capacitance–voltage (CV) measurements at 300 K and 77 K, using an HP4284A LCR meter, within the frequency range 1 kHz–1 MHz, after evaporating Al electrodes on top of the top oxide (TOX) and a blanket Al layer on the wafer backside and sidewalls to ensure a reliable contact to the  $\text{Ge}_x\text{Si}_{1-x}$  layer. When this MOS structure is polarized to accumulate charges in the  $\text{Ge}_x\text{Si}_{1-x}$  layer, the measured capacitance corresponds to the capacitance  $C_{\text{TOX}}$  of the TOX. However, when the active  $\text{Ge}_x\text{Si}_{1-x}$  layer is depleted, mobile carriers are unable to respond to the ac probing signal and a decrease in the measured capacitance is observed [8]. The transition between these two states is observed as a drop of the capacitance from which we can infer a “threshold” voltage ( $V_T$ ) that is related to the amount of interface charges ( $Q = V_T C_{\text{TOX}}$ ) as shown in Fig. 1; more precisely,  $V_T$  is defined as the gate voltage at which the total capacitance has dropped by 10% relative to the accumulation value. The direction of the CV curve voltage shift indicates that the observed defects are

negatively charged. By using etch-back experiments, not discussed here, we established that no significant charge density is present in the  $\text{SiO}_2$  layers. This result indicates that negative charges are mostly located at the  $\text{Ge}_x\text{Si}_{1-x}/\text{SiO}_2$  interfaces.

Electron spin resonance (ESR) measurements were performed in a K-band (20.5 GHz) spectrometer at 4.3 K to evaluate the density of  $\text{GeP}_{b1}$  centers as a function of Ge concentration. A co-mounted Si:P marker sample [ $g(4.2\text{ K}) = 1.99869$ ] was used for  $g$ -value calibration and defect density determination.

Positron annihilation spectroscopy (PAS) in the Doppler broadening mode was applied to independently detect negatively charged Ge DB centers [8]. The set-up used for these experiments employed a monoenergetic positron beam emitted by a moderated  $^{22}\text{Na}$  source. The annihilation  $\gamma$ -rays (of photon energy  $E_\gamma = 511$  keV) were detected using a high-purity Ge detector with a resolution of 1.3 keV at 511 keV. The line shape parameters ( $S$ ,  $W$ ) are defined as the fraction of counts in the central window ( $S$ ) and in the wings ( $W$ ) of the annihilation peak with respect the total number of counts. The  $S$  parameter energy window was chosen in the typical range  $|E_\gamma - 511\text{ keV}| < 0.83$  keV symmetrically around the peak of the energy distribution of the annihilation photons  $E_\gamma$ . The  $W$  parameter was evaluated from the wings of the annihilation peak distribution symmetrically in the range  $3.00\text{ keV} < |E_\gamma - 511\text{ keV}| < 7.60$  keV. More details on the data analysis can be found elsewhere [12,13].

## 3. Results

### 3.1. Effect of strain

As reported by Souriau et al. [11], the lattice constant of the  $\text{Ge}_x\text{Si}_{1-x}$  alloy increases with Ge content, while oxidation of Si to  $\text{SiO}_2$  increases the molar volume of the material. As a consequence,

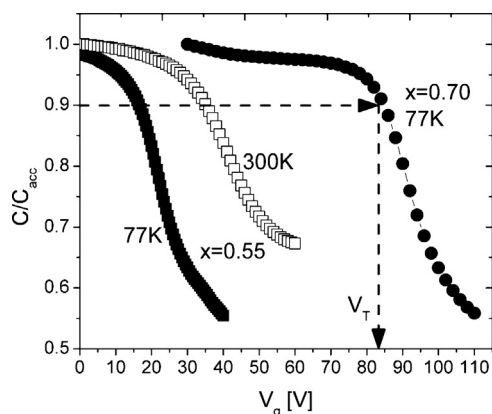


**Fig. 1.** 100 kHz CV curves measured at 300 K and 77 K (empty and full symbols, respectively) in samples containing different concentrations of Ge in the  $\text{Si}_{1-x}\text{Ge}_x$  layer. The inferred “threshold” ( $V_T$ ) is defined as the gate voltage at which the total capacitance drops by 10%.

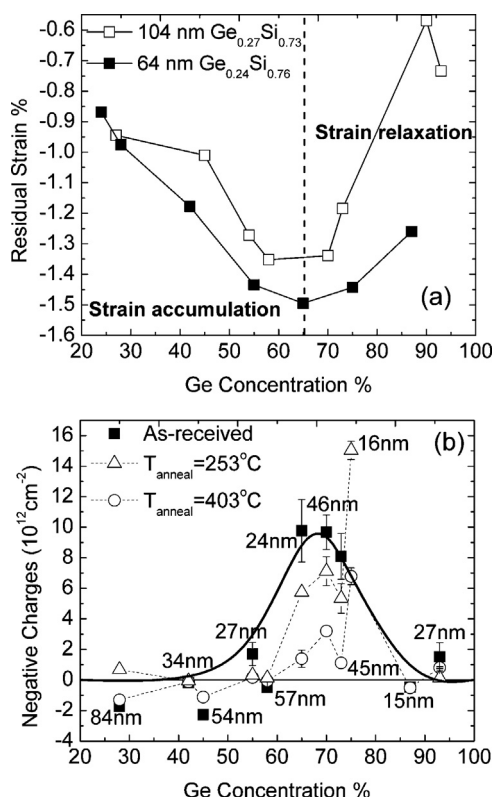


**Fig. 2.** (a). Residual strain in  $\text{Ge}_x\text{Si}_{1-x}$  layers as a function of Ge content in samples fabricated by the condensation of germanium starting from different thicknesses of the initial  $\text{GeSi}$  films (i.e., 104 nm and 64 nm, as indicated) as measured by HR-XRD. The Ge concentrations were determined by RBS. (b) Charge density determined from the CV curves at 77 K in the as-received samples (■) and in the samples passivated by annealing in  $\text{H}_2$  for 30 min at 253 °C (Δ) and 403 °C (○) as a function of Ge concentration. The thicknesses of the  $\text{Si}_{1-x}\text{Ge}_x$  layers obtained from HR-XRD scans are indicated for each sample. The bold solid curve and dotted lines guides the eye.

during the condensation process the  $\text{Ge}_x\text{Si}_{1-x}$  layer experiences high levels of stress that leads to generation of extended imperfections and (interface) point defects allowing the  $\text{Ge}_x\text{Si}_{1-x}$  layer to partially accommodate the mismatch with the TOX and BOX layers.

The results of strain measurements using HR-XRD are plotted in Fig. 2(a) as a function of Ge concentration. Starting from low Ge concentration ( $x \leq 0.25$ ) the inferred residual strain in  $\text{Ge}_x\text{Si}_{1-x}$ , in absolute values, increases with  $x$  to reach a maximum at around  $x = 0.68$ . For higher concentrations a relaxation of the strain is observed which was found to correlate with generation of dislocations in the  $\text{Ge}_x\text{Si}_{1-x}$  layer. Also observed is a substantial dependence on the thickness of the  $\text{Ge}_x\text{Si}_{1-x}$  layer itself: In the second set of samples [filled squares in Fig. 2(a)], fabricated from a thinner initial  $\text{Ge}_x\text{Si}_{1-x}$  layer (64 nm thick) than the first set of samples (open squares in Fig. 2(a); 104 nm thick initial  $\text{Ge}_x\text{Si}_{1-x}$  layer), an overall increase in residual strain of  $\approx 0.2\%$  is found, indicating that strain relaxation is more difficult than for a thicker  $\text{Ge}_x\text{Si}_{1-x}$  layer of the same composition.

The areal density of negative charges as a function of Ge fraction has been monitored both in the as-received samples and after two different passivation anneals for  $30 \pm 1$  min in 1 atm  $\text{H}_2$ . At the chosen anneal temperatures of 253 °C and 403 °C we were able to passivate between 50% and 93% (depending on  $x$ ) of the defects in the first set of samples used in this work (numbers 1–5 in Table 1) [14], as can be seen from the defect densities shown in Fig. 2(b). The CV measurements performed on the  $x = 0.75$  sample (number 10 in Table 1) in the as-received state did not allow us to reach depletion in the GeSi layer because of TOX dielectric breakdown. Nevertheless, by making use of the observed breakdown voltage, we were

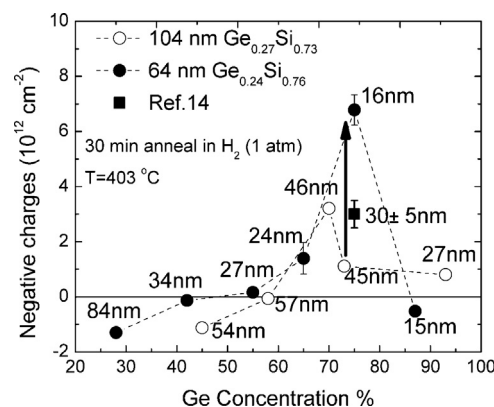


**Fig. 3.** Density of charge evaluated after passivation in  $\text{H}_2$  for 30 min at 403 °C in the samples prepared from a thinner (●) and thicker (○) initial starting  $\text{Ge}_x\text{Si}_{1-x}$  layer, as indicated in the figure. Data from Ref. [14] is included. The arrow indicates the effect associated with an increased residual strain in terms of density of defects resistant to passivation by hydrogen.

able to estimate the lower limit of the density of negative charges at the  $\text{Ge}_x\text{Si}_{1-x}/\text{SiO}_2$  interfaces in this sample as  $1.8 \times 10^{13} \text{ cm}^{-2}$ .

Several results suggest the influence of the residual strain on the formation of the observed defects and their passivation by hydrogen. First, with respect to the as-received samples, we notice from Figs. 2(a) and (b) that starting from a minimum defect density in the Si-rich samples, the maximum charge density is reached when the  $\text{Ge}_x\text{Si}_{1-x}$  layer is strained to the maximum [in the range ( $0.6 < x < 0.8$ )]. Both the strain and the charge density are seen to decrease for higher Ge concentrations, suggesting that both phenomena may be governed by a common physical mechanism.

Second, the data show that the generation of negative charges is enhanced by a relatively small increment of the residual strain in the  $\text{Ge}_x\text{Si}_{1-x}$  layer. A representative case is provided by the samples listed in Table 1 as numbers 4 and 10. While both are characterized by nearly the same Ge content ( $x = 0.73$  and  $0.75$ , respectively), the thickness of the  $\text{Ge}_x\text{Si}_{1-x}$  layer in the second sample is smaller by a factor of  $\sim 3$  (16 nm versus 45 nm). The thinner  $\text{Ge}_x\text{Si}_{1-x}$  layer leads to an increase in negative charge density from  $8.1 \times 10^{12} \text{ cm}^{-2}$  to more than  $1.8 \times 10^{13} \text{ cm}^{-2}$ , as evaluated from the breakdown voltage, which can be correlated with the increase of the residual strain as shown in Fig. 2(a).

Finally, analysis of defect densities in the samples with different degree of hydrogen passivation (open triangles and circles in Fig. 2(b)) suggests that the strain may severely reduce the efficiency of the passivation treatment. By comparing the densities of negative charges found in the two sets of samples with different thickness of the initial  $\text{Ge}_x\text{Si}_{1-x}$  layer after annealing in hydrogen for 30 min at 403 °C (Fig. 3), we can see that the amount of defects resistant to the passivation is enhanced in the samples with a thinner initial  $\text{Ge}_x\text{Si}_{1-x}$  film. For example, in the already discussed samples (number 4 and 10), the density of unpassivated defects is different by a factor of  $\sim 7$ , as indicated by the bold arrow in Fig. 3.

### 3.2. Assessment of the defects

ESR measurements were able to probe the paramagnetic centers at both interfaces of the  $\text{Ge}_x\text{Si}_{1-x}$  layers with  $\text{SiO}_2$ . Field angular dependent measurements revealed a g-map much reminiscent of that of the well-known  $\text{SiP}_{\text{b1}}$  centers found in (100)Si/ $\text{SiO}_2$  [6]. However, the generally much larger (more extreme g matrix) g-values indicate these centers to originate from unpaired electrons localized at defected Ge atoms at the  $\text{Ge}_x\text{Si}_{1-x}/\text{SiO}_2$  interfaces. These results, together with other ESR attributes, led to the modeling of the defect as  $\text{Ge P}_{\text{b1}}$  center [6,7,15].

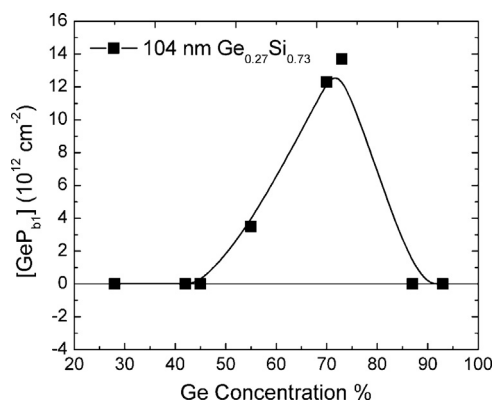


**Fig. 4.** Areal density per  $\text{cm}^{-2}$  of sample as a function of Ge concentration of paramagnetic  $[GeP_{b1}]$  centers in condensation grown  $(100)\text{Si}/\text{SiO}_2/\text{Ge}_x\text{Si}_{1-x}/\text{SiO}_2$  structures starting from an initial 104 nm thick  $\text{Ge}_{0.27}\text{Si}_{0.73}$  layer. The curve guides the eye. Additional data points have been added according to Refs. [6,8].

As already reported [8] and confirmed in the present work, the density of paramagnetic  $GeP_{b1}$  centers, shown in Fig. 4, as a function of Ge content matches quantitatively the density of observed negative charges. The p-type conductivity of the  $\text{Ge}_x\text{Si}_{1-x}$  layer and the temperature-induced shift of the CV curves (the Grey-Brown shift) observed when cooling down the samples from room temperature to the boiling point of nitrogen (77 K), illustrated in Fig. 1, suggest these defects to be acceptors [8]. Such a correspondence between a singly occupied paramagnetic DB ( $GeP_{b1}$  defect) and a negatively charged center which means capture of an additional electron needs additional analysis.

Apparently, at 77 K most of the  $GeP_{b1}$  centers are negatively charged because their energy level is still below the Fermi level in  $\text{Ge}_x\text{Si}_{1-x}$  [16]. However, when cooling the sample down to 4.2 K, the GeSi Fermi level moves toward the valence band (VB) edge. As a consequence, one may suggest that most of the defects turn neutral. To verify this hypothesis one needs to find an experimental method capable of tracing the behavior of the negatively charged defects in the temperature range from below 77 K to room temperature. For this reason, we invoked PAS as the technique that might sense the negatively charged centers.

In the first step, using PAS experiments performed at room temperature, we were able to establish that the examined interfacial defects constitute a trapping site for positrons. Furthermore, by tracing the effect of annealing in  $\text{H}_2$ , PAS can provide experimental evidence that the presence of a negative charge is associated with the availability of unpassivated defects.

The Doppler broadening measurements performed in this work sense the momentum of the annihilating electron-positron pair through a broadening of the 511 keV annihilation  $\gamma$ -line [12,13,17,18]. This effect is quantified using the line shape parameters  $S$  and  $W$ , referred to also as low and high momentum parameters. Manifestations of separate trapping states may arise in the  $(S, W)$  plane as clusters of closely gathered  $(S_i, W_i)$  points. In presence of only two annihilation states (e.g., at the surface and in the bulk of the sample) the measured parameters can be described as a superposition of the  $S_i$  and  $W_i$  parameters of these two single positron trapping states. As a result, with increasing positron implantation energy, one will find the  $S, W$  values along a straight line connecting two characteristic states in the  $(S, W)$  plane. A non-linear behavior observed in this plot will then indicate the presence of additional annihilation states.

The results obtained for sample 10 ( $x=0.75$ ) without and after passivation in hydrogen are shown in Fig. 5(a), where the solid curve indicates the flow in measurements sequentially performed with increasing positron implantation energy. At low implantation

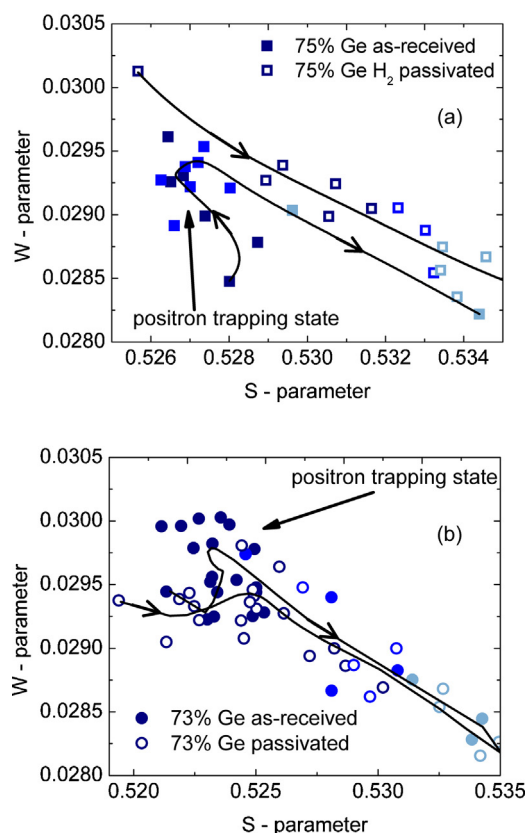


**Fig. 5.** (a) and (b) The positron annihilation spectra ( $S, W$ ) parameters measured in the samples containing 75% (■, □) and 73% (●, ○) of Ge in the  $\text{Ge}_x\text{Si}_{1-x}$  layer prior and after passivation by  $\text{H}_2$ . Solid curves mark the flow in measurements with increasing positron implantation energies.

energies, a clustering of points can be seen in the as-received sample (filled squares), providing evidence for the existence of a specific trapping state [12,13]. This state disappears after the (DB) passivation treatment in  $\text{H}_2$  (open squares) confirming that the detected state arises from the interfacial defects observed electrically and by ESR. In Fig. 5(b) the similarly obtained  $S$ - $W$  plot is shown for the sample with  $x=0.73$  (sample 4). Also in this sample the  $(S, W)$  pairs measured at low implantation energies aggregate in the same region of the  $(S, W)$  plane. However, because of the lower density of negative charges present in this sample than in number 10 [c.f. Fig. 2(b)] and, as a result, a lower sensitivity of the PAS technique to this particular positron trapping site, the resulting cluster is spread over a larger area. Nevertheless, a similar change in the  $S$ - $W$  trend is found after passivation [open circles in Fig. 5(b)] as for sample 10 and, taking into account the similarity of these results to the data shown in Fig. 5(a), there is a clear indication that the same positron trapping state is present in sample 4 ( $x=0.73$ ) and in sample 10 ( $x=0.75$ ).

In Fig. 6, the inferred value of the  $S$  parameter is shown as a function of the positron implantation energy (which is linearly related to the mean implantation depth) for samples 4 and 10 before and after passivation  $\text{H}_2$ . At the acceleration energies close to 2 keV, we are able to implant positrons to a mean depth of  $\sim 180$  nm, i.e., close to the top  $\text{SiO}_2/\text{Ge}_x\text{Si}_{1-x}$  interface. For positron implantation energies  $\leq 2.5$  keV a plateau, in  $S$ -parameter, is observed in both samples in the as-received (unpassivated) state, indicating the presence of a trapping site that reduces the diffusion length of positrons. Upon passivation of the defects, a change in the  $S$ -energy relationship becomes clearly seen in this region as a monotonic increase of the  $S$ -values with increasing acceleration energy. This result suggests that



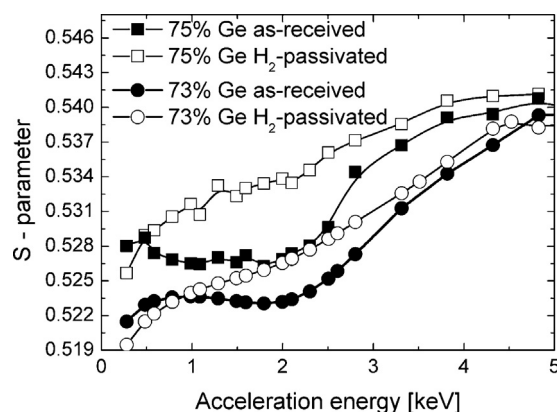


**Fig. 6.** *S* parameters as a function of positron implantation energy as measured in samples containing thin 75% (■, □) and thick 73% (●, ○) of Ge in the  $\text{Ge}_x\text{Si}_{1-x}$  layer, prior and after passivation in  $\text{H}_2$ .

by attaching hydrogen atoms to the DBs, the latter become inactive as positron traps. As a result, the positrons implanted with an acceleration energy lower than  $\sim 5$  keV will get a larger diffusion length, leading to the observed gradual increase of the measured *S* value from that characteristic of surface positron trapping, to the value typical for positron annihilation in the bulk of the silicon substrate.

#### 4. Conclusions

In this work we have shown that the residual strain represents an important factor influencing the quality of the  $\text{Ge}_x\text{Si}_{1-x}/\text{SiO}_2$  interface in terms of occurring charge traps. There are two major effects: First, the initial density of dangling bond defects,  $\text{GeP}_{\text{b1}}$  centers, acting as shallow acceptors in  $\text{Ge}_x\text{Si}_{1-x}$ , increases with increasing residual strain. Second, the efficiency of passivation of these defects by annealing in hydrogen decreases in samples with highly strained  $\text{Ge}_x\text{Si}_{1-x}$  layers leaving up to 40% of these traps resistant to the passivation. These observations are corroborated by PAS observations indicating the negatively charged defects to be efficient positron traps. The latter enables one to use PAS in order to monitor the density of active (negatively charged) states irrespectively of the conductivity of the Si substrate. This approach will be used in the future to analyze the temperature-induced variations in DB charge states.

#### Acknowledgments

This work has received financial support from the EU FP7 project MORDRED (Grant No. 261868) and COST European Cooperation in Science and Technology, action CM1104 “Reducible oxides”.

#### References

- [1] N.H. Thoan, K. Keunen, V.V. Afanas'ev, A. Stesmans, Interface state energy distribution and  $\text{P}_{\text{b}}$  defects at  $\text{Si}(110)/\text{SiO}_2$  interfaces: comparison to (111) and (100) silicon orientations, *J. Appl. Phys.* 109 (2011) 013710.
- [2] V.V. Afanas'ev, Y.G. Fedorenko, A. Stesmans, Interface traps and dangling-bond defects in  $(100)\text{Ge}/\text{HfO}_2$ , *Appl. Phys. Lett.* 87 (2005) 032107.
- [3] F. Bellenger, M. Houssa, A. Delabie, V. Afanas'ev, T. Conard, Passivation of  $\text{Ge}(100)/\text{GeO}_2/\text{high-k}$  gate stacks using thermal oxide treatments, *J. Electrochem. Soc.* 155 (2008) G33–G38.
- [4] C.H. Lee, T. Tabata, T. Nishimura, K. Nagashio, K. Kita, A. Toriumi,  $\text{Ge}/\text{GeO}_2$  interface control with high-pressure oxidation for improving electrical characteristics, *Appl. Phys. Exp.* 2 (2009) 071404.
- [5] M. Fanciulli, A. Molle, S. Baldovino, A. Vellei, Magnetic resonance spectroscopy of defects at the dielectric-semiconductor interface: Ge substrates and Si nanowires, *Microelectron. Eng.* 88 (2011) 1482–1487.
- [6] A. Stesmans, P. Somers, V.V. Afanas'ev, Electron spin resonance observation of an interfacial  $\text{GeP}_{\text{b1}}$ -type defect in  $\text{SiO}_2/(100)\text{Si}_{1-x}\text{Ge}_x/\text{SiO}_2/\text{Si}$ , *J. Phys. Condens. Mater.* 21 (2009) 122201.
- [7] A. Stesmans, P. Somers, V.V. Afanas'ev, Nontrigonal Ge dangling bond interface defect in condensation-grown  $(100)\text{Si}_{1-x}\text{Ge}_x/\text{SiO}_2$ , *Phys. Rev. B* 79 (2009) 195301.
- [8] V.V. Afanas'ev, M. Houssa, A. Stesmans, L. Souriau, R. Loo, Electronic properties of Ge dangling bond centers at  $\text{Si}_{1-x}\text{Ge}_x/\text{SiO}_2$  interfaces, *Appl. Phys. Lett.* 95 (2009) 222106.
- [9] B. Vincent, J. Damlencourt, V. Delaye, R. Gassilloud, L. Clavelier, B. Vincent, J. Damlencourt, V. Delaye, R. Gassilloud, L. Clavelier, Stacking fault generation during relaxation of silicon germanium on insulator layers obtained by the Ge condensation technique, *Appl. Phys. Lett.* 90 (2007) 074101.
- [10] L. Souriau, V. Terzieva, W. Vandervorst, F. Clemente, B. Brijs, A. Moussa, M. Meuris, R. Loo, M. Caymax, High Ge content SGOI substrates obtained by the Ge condensation technique: a template for growth of strained epitaxial Ge, *Thin Solid Films* 517 (2008) 23–26.
- [11] L. Souriau, T. Nguyen, E. Augendre, R. Loo, V. Terzieva, M. Caymax, S. Cristoloveanu, M. Meuris, W. Vandervorst, High-hole-mobility silicon germanium on insulator substrates with high crystalline quality obtained by the germanium condensation technique, *J. Electrochem. Soc.* 156 (2009) H208–H213.
- [12] J. Slotte, F. Tuomisto, Advances in positron annihilation spectroscopy of Si, Ge and their alloys, *Mater. Sci. Semiconductor Process.* 5 (2012) 669–674.
- [13] M. Clement, J. DeNijs, P. Balk, H. Schut, A. VanVeen, Analysis of positron beam data by the combined use of the shape- and wing- parameters, *J. Appl. Phys.* 79 (1996) 12.
- [14] N. Thoan, A. Stesmans, P.D. Nguyen, K. Keunen, V.V. Afanas'ev, Chemical kinetics of the hydrogen- $\text{GeP}_{\text{b1}}$  defect interaction at the  $(100)\text{Ge}_x\text{Si}_{1-x}/\text{SiO}_2$  interface, *J. Vacuum Sci. Technol. B* 31 (2013), 010603-1.
- [15] P. Somers, A. Stesmans, L. Souriau, V.V. Afanas'ev, Electron spin resonance features of the  $\text{GeP}_{\text{b1}}$  dangling bond defect in condensation-grown  $(100)\text{Si}/\text{SiO}_2/\text{Si}_{1-x}\text{Ge}_x/\text{SiO}_2$  heterostructures, *J. Appl. Phys.* 112 (2012) 074501.
- [16] M. Houssa, V.V. Afanas'ev, A. Stesmans, G. Pourtois, M. Meuris, First-principles study of the electronic properties of Ge dangling bonds at  $(100)\text{Si}_{1-x}\text{Ge}_x/\text{SiO}_2$  interfaces, *Appl. Phys. Lett.* 95 (2009) 162109.
- [17] S. Kilpelainen, Y.-W. Lu, F. Tuomisto, J. Slotte, A.N. Larsen, Si nanoparticle interfaces in  $\text{Si}/\text{SiO}_2$  solar cell materials, *Condens. Matter Mater. Sci.* (2011) arXiv:1106.1753v1.
- [18] R.W. Siegel, Positron annihilation spectroscopy, *Ann. Rev. Mater. Sci.* 10 (1980) 393–425.